ISSN 1063-7710, Acoustical Physics, 2023, Vol. 69, No. 1, pp. 58–73. © The Author(s), 2023. This article is an open access publication.

PHYSICAL ACOUSTICS

Slow Time Phenomena in Heterogeneous Materials: from Microscopic Fluctuations to Macroscopic Relaxation

A. V. Lebedev[a, *]

[a] *Institute of Applied Physics, Nizhny Novgorog, 603950 Russia*

**e-mail: swan@appl.sci-nnov.ru*

Received June 14, 2022; revised June 14, 2022; accepted September 22, 2022

Abstract—Slow time relaxation of elastic moduli with typically logarithmic time dependence is observed in many media interesting for materials science. This phenomenon is related to internal structure and is, hence, important for the development of present-day materials. Here, we provide a general explanation showing a close link between slow time phenomena and fluctuations on the microscopic and mesoscopic scales. We look for the origin of slow time phenomena in random walk or diffusion processes on microscopic scales. Some bonds occurring in the metastable state make a transition through the energy barriers due to small fluctuations slightly perturbing the statistical equilibrium. If the number of the excited bonds is small compared to the total number of bonds in a heterogeneous material, the process of the transition as a whole can be considered as mesoscopic fluctuations. Averaging over all transient bonds or states is revealed in the observed macroscopic relaxation of elastic moduli, velocities, and others. The functional dependence on time in the relaxation process has been shown to be controlled by the profile of energy barriers. The results obtained point to their possible applications in materials science.

Keywords: slow time relaxation, fluctuations, diffusion, Fokker–Planck equation

DOI: 10.1134/S1063771022700543

1. INTRODUCTION

The response of solids to finite deformation is of great interest in materials science. The nonlinearity of a solid medium arising at small deformations has been known since the 19-th century when experimentalists showed an approximate character of Hooke's law for many materials [1, Para 2.2] or (see paragraph 2.2 in [1]). A thermodynamic definition of this nonlinearity was given in [2, 3] and was related to the Taylor expansion of the free energy of elastic deformation. The coefficients of the quadratic terms of strain tensor correspond to the linear elastic moduli entering Hooke's law, while the higher-order terms correspond to physical nonlinearity. These coefficients reveal the properties of bonds between atoms, which is useful for materials science applications. A comprehensive historical review of classical results is presented in the [4]. A solid review of the theoretical background can be found in Chapter 2 of [5]. This type of nonlinearity is regarded to be classical [6–8].

It is well known that materials with a complex internal structure (e.g., composites, ceramics, building materials) are characterized by acoustic nonlinearity which is anomalous compared to homogeneous materials (metals, crystals, and others) [9]. In this case, deviations from Hooke's law for the stress–strain relation manifest themselves significantly not only in values of higher elastic moduli but also in hysteresis and relaxation processes. The interactions between the structural elements in heterogeneous solids greatly differ from those in homogeneous ones, where bonds are associated with atomic forces, energies, and so on [5]. The unusual properties of heterogeneous materials due to contacts of various scales (structural nonlinearity [9]) allowed distinguishing them as a separate class [10]. Rocks (natural building materials) are the most vivid example of heterogeneous media with strong acoustic nonlinearity in view of a variety of spatial scales of structural inhomogeneity formed over a long (geological) time. Analogous properties are attributed to artificial materials with a complex internal structure, such as cement, concrete, damaged ceramics and glasses, etc., which enables nonlinear evaluation of internal structure integrity [5, 9–14]. Two phenomena have been observed separately or together: hysteresis in the stress-strain relation and long-time relaxation. The first phenomenon was defined in [5] as a fast time process, the second one as a slow time process. Numerous experimental results were systematized and discussed in [5, 8]. Slow relaxation phenomena are observed in absolutely different materials, both natural and artificial on various scales [5, 10, 14–20], even on large scales, like for earthquakes [21–23].

The first qualitative model of an intriguing slow time relaxation phenomenon was proposed and compared with the experimental data in [15]. The authors

supposed that strong deformations during external periodic loading (conditioning in terms of [5, 10, 15]) result in something equivalent to a frictional slip, as a system of broken bonds is created. The logarithmic relaxation was interpreted as the integral over a smooth distribution of the activation energies with a wide spectrum of values. The model [15] was successfully used for studying the complex kinetics of oil viscosity in [19, 20]. By analogy with the theory of relaxation losses in fluids (see §81 in [24]), in [19] the viscous media were assumed to be controlled by an internal parameter characterized by the activation energy similar to [15]. Solution of the Arrhenius type equation provides a logarithmic time dependence for the viscoelastic properties of the studied oils. Numerous experimental data are presented in [19, 20]. A thermoelastic mechanism of slow relaxation was proposed in the paper [25]. The initial bond breaking was related to the nonlinear effect of strain rectification, while the subsequent slow time relaxation was explained by thermally activated microscopic strains with a wide spectrum of characteristic times of thermal diffusion. The data presented demonstrate that both conditioning and relaxation have the same logarithmic dependence on time. The authors of [26] considered a package of smooth glass balls with adhesion between them. They assumed that high-intensity conditioning ruptures week bonds. Each bond is related to individual surface energy and barriers, creating their wide spectrum. After numerical simulation, actually analogous to the direct integration made in [15], relaxation with logarithmic dependence on time was shown. The correlation between fast and slow motions was pointed in [27], although the time scales for conditioning and relaxation processes were different contrary to [25]. The authors of that paper treated the slow time relaxation as non-equilibrium behavior (see also [28]). Then they noted: "it is not clear whether a single universal mechanism or, rather, a specific material-dependent one should be identified as the origin of nonlinearity and non-equilibrium behavior".

A physical model explaining the origin of both hysteresis nonlinearity and slow time relaxation in a heterogeneous medium was proposed in [29]. A heterogeneous medium within the framework of this model is considered as a number of grains bonded by surface forces of different nature [30]. According to [30, 31], the interaction potential of rough contacts is a non-monotonous function $V(h)$, where h is the distance between the nearest points of contacting surfaces. This potential has at least two equilibrium states (see examples in [31]) separated by barrier(s): $h = h_p$ with $V(h_p) = V_p$ corresponds to the main equilibrium state, and $h = h_s$ with $V(h_s) = V_s > V_p$ corresponds to the secondary equilibrium state. If a detached bond is close enough to the main equilibrium state, the attaching–detaching processes provide nonlinear hysteresis phenomena (a well-grounded phenomenological description is presented in [5, 32]). If a detached bond is in the secondary minimum of the surface potential and the barrier height is more than the kinetic energy of thermal motions, then this bond is in a metastable state with slow time relaxation. Slow relaxation was presumably related for the first time to metastable states inside solids in [16], where the observed logarithmic dependence was explained using the Arrhenius law for the local strain rate, and macroscopic description was used.

Here we will show how the logarithmic time dependence originates from microscopic fluctuations due to random walking (diffusion). On the macroscopic scale, a logarithmic time dependence arises as a result of averaging over bonds in metastable states. Each bond can be considered as a structural element on a mesoscopic or an intermediate scale. Thus, we interpret slow time phenomena as multi-scale fluctuations. The models proposed can be used in materials science to evaluate the properties of promising materials.

The paper is organized as follows. Section 2 provides a brief description of the basic results of [29]. The previously overlooked issue of the transition of a detached bond to a metastable state is also explained in this section. Section 3 describes the used surface potential. Preliminary estimates of the characteristic distances between two contacting surfaces are also given in this section. In Section 4 we describe microscopic fluctuations that lead to slow relaxation but are not logarithmic in time. In Section 5 the fluctuation of each metastable contact is considered on a mesoscale (individual adhesive bonds) as a limiting case of binomial distribution for all bonds in the heterogeneous material. We will show in this section that, under some reasonable assumptions, it is possible to obtain a logarithmic time dependence for relaxing elastic moduli. Section 5 also provides the description of the excitation stage pointing to the reversibility in excitation/relaxation processes and possible kinetic effects in the excitation process. The results obtained are discussed in Section 6 and are compared with known experimental data, confirming the proposed theoretical description. The conclusions are formulated in Section 7.

2. PRELIMINARY ESTIMATIONS

The adhesion hysteresis occurs when the adhesion layer stiffness is higher than that of curved elastic bodies in contact (grains, roughness, and so on). Mathematically this is formulated as $\mu > 1$, where the dimensionless parameter [33] is

$$\mu = \left(\frac{V_p^2 R}{\tilde{E}^2 h_p^3}\right)^{1/3}, \qquad (1)$$

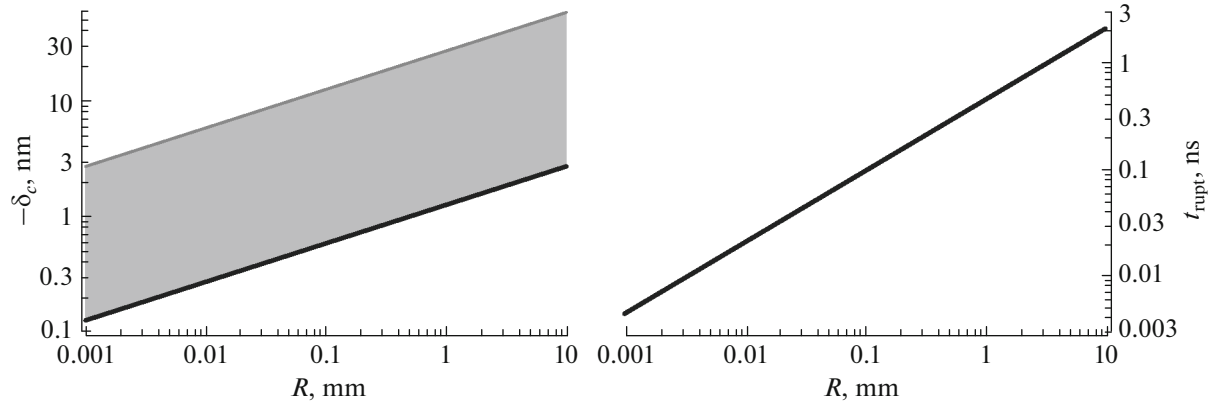

Fig. 1. On the left: the dependence (4) of $-\delta_c$ on curvature radius R for glass balls with $\gamma = -V_p = 0.1$ J/m^2. The gray line and area depict the influence of dissipative effects on $-\delta_c(R)$. On the right: estimate of contact detachment time

where $R = \left(1/R_1 + 1/R_2\right)^{-1}$ is the equivalent curvature radius of two elastic bodies (e.g., balls) with curvature radii $R_{1,2}$, $\tilde{E} = \left(\frac{1-\nu_1^2}{E_1} + \frac{1-\nu_2^2}{E_2}\right)^{-1}$ is the effective Young modulus of two contacting bodies [34], and $E_{1,2}$ and $\nu_{1,2}$ are the Young modulus and the Poisson ratio of each body. According to the numerical simulations, the adhesion hysteresis occurs if $\mu \gtrsim 1$ [33, 35]. If $\mu \ll 1$ there is no hysteresis; in this case, the contact is broken and is restored at the same separation distance h between the nearest points of the contacting bodies. If $\mu \gg 1$, adhesion hysteresis manifests itself as a difference in h for contact breaking and restoration. In this case, the contact of two deformable bodies with adhesion between them is described by the model proposed in [36]. Here we use the expressions from [35] that are more convenient than the ones presented in [36]:

$$F = \frac{4\tilde{E}a^3}{3R} - \sqrt{8\pi\gamma\tilde{E}a^3},$$
$$\delta = \frac{a^2}{R} - \frac{2}{3}\sqrt{\frac{9\pi\gamma a}{2\tilde{E}}}, \quad (2)$$

where F is the external force pressing two balls together, a is the contact radius, δ is the variation of the distance between the ball centers, $\gamma = -V_p$ is the adhesion coefficient. The thickness of the adhesion layer within the framework of the model [36] is assumed to be zero (adhesion layer stiffness is infinite).

The bond strength or force F_b required to break the contact is determined by the adhesion coefficient γ (material parameter) and curvature R of two contacting bodies (geometrical parameter):

$$F_b = -3\pi\gamma R/2, \quad (3)$$

where the "–" sign corresponds to the force of ball detachment. In the absence of adhesion ($\gamma = 0$), the contact of two elastic bodies is described by Hertz's theory [34] and body detachment occurs at $F_b = 0$. When the condition ((3)) is fulfilled, the values of a and δ are

$$a_c = \left(\frac{9\pi\gamma R^2}{8\tilde{E}}\right)^{1/3},$$
$$\delta_c = -\frac{1}{12}\left(\frac{9\pi\gamma}{\tilde{E}}\right)^{2/3} R^{1/3}. \quad (4)$$

Here, the negative value of δ_c corresponds to detachment. When the contact is restored, $a = \delta = 0$.

Under uniform displacement x in a heterogeneous medium, the local strain level $\epsilon \simeq x/R$ may be insufficient to break bonds with $\mu > 1$. Therefore, as was shown in [29], the transition from classical nonlinearity to nonlinear hysteresis has a threshold in the strain level. This was first shown experimentally in [28]. Later a more rigorous experimental study was performed [18], showing also the dependence of the threshold mentioned on environmental conditions (water content in porous space). The threshold value of strain was estimated to be $\epsilon_t \sim 10^{-7}$ in [29], which is in a good agreement with the measured values [18, 28]. Within the framework of the model presented in [29] we postulated that some broken contacts moved to the secondary minimum where $\mu \ll 1$. Therefore, such contacts no longer participated in the fast motions and no hysteresis including contact restoration occurred for them. The transition to a metastable state was not described in [29], so it will be considered in what will follow.

The value of $\delta_c < 0$ corresponds to the beginning of instability when contact breaks. The instability occurs

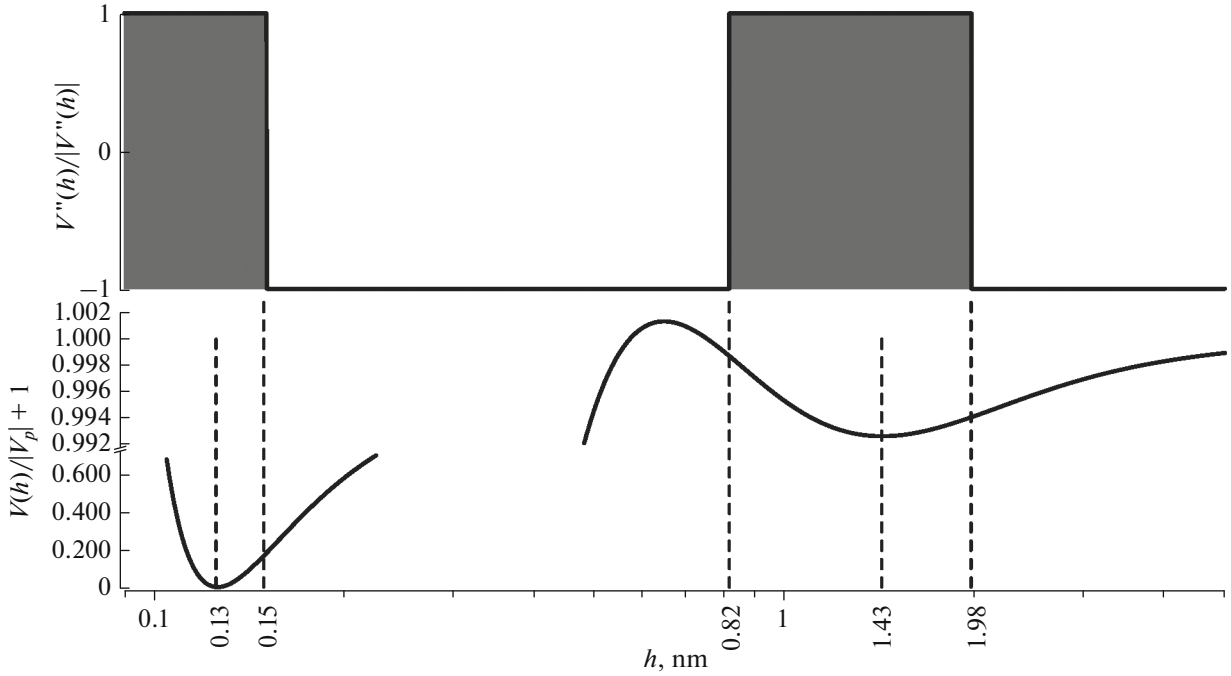

Fig. 2. An example of potential function ((5)) for $\rho = 0.08\rho_{max}$ and $\psi = 0.5$ V. The upper plot depicts the sign of the second derivative $\partial^2 V(h)/\partial h^2$.

when the sum of elastic and surface energies has a non-positive quadratic form [36]. After contact breaking, the separation distance $h = -\delta_c$. If this value is close enough to the basin of attraction of the secondary minimum of the surface potential $V(h)$, the broken contacts are in the metastable state. An example of the dependence of $-\delta_c$ on curvature radius for glass balls is presented in the left graph in Fig. 1.

All the above considerations do not take into account kinetic effects which are very important in adhesive bonds breakage. It is well known that the dissipative processes play an important role, leading to an increase in the effective value of the adhesion coefficient γ by up to two orders of magnitude [37–39]. The value of δ_c is proportional to $\gamma^{2/3}$ (4). The corresponding corrections due to dissipative processes are depicted by the gray line and the light-gray area. Below it is shown that the values of δ_c plotted in Fig. 1 really correspond to the attraction area of the secondary minimum of surface potential $V(h)$.

Although kinetic effects are difficult to describe [38], the speed of adhesive bond breaking is known to be limited by Rayleigh wave velocity [39]. Therefore, the time of the contact rupture t_{rupt} can be estimated as a time required for the Rayleigh wave to pass a distance of $2a_c$. The result of the corresponding calculations, with adhesion coefficient multiplied by 100 to take into account the dissipative effects, is presented on the right of Fig. 1. The highest frequency used for initiating slow time relaxation was about $\omega/2\pi \sim 100$ kHz [14]. The product $\omega t_{rupt} \lesssim 10^{-3}$ (Fig. 1, right) is obviously much less than unity, which means an early instant transition of the broken contact in metastable state, if other conditions are fulfilled.

3. MODEL OF SURFACE POTENTIAL

As pointed above, the potential of surface forces usually has several secondary minima (see examples in [31]). For the sake of simplicity, we consider the model potential known as the DLVO potential which has an analytical form [30]:

$$V(h) = -\frac{A}{12\pi h^2}\left[1 - \left(\frac{h_0}{h}\right)^6\right] + BkT\exp\left(-h/\lambda_D\right),$$
$$B = 64\rho\zeta_1\zeta_2\lambda_D, \quad \text{and} \quad \lambda_D = \sqrt{\frac{\varepsilon_0\varepsilon kT}{2q_e^2\rho}}, \tag{5}$$

where h is the separation distance between the interacting surfaces, $A = 10^{-20}$–10^{-19} J is the Hamacker constant, $k = 1.38\times10^{-23}$ J/K is the Boltzmann constant, T is absolute temperature, and $h_0 \simeq 10^{-10}$ m is the characteristic atomic size. The second term in square brackets describes strong repulsion of atoms (see [30] for details). The factor B in the last term of (5) depends on the ion concentration ρ, surface charge

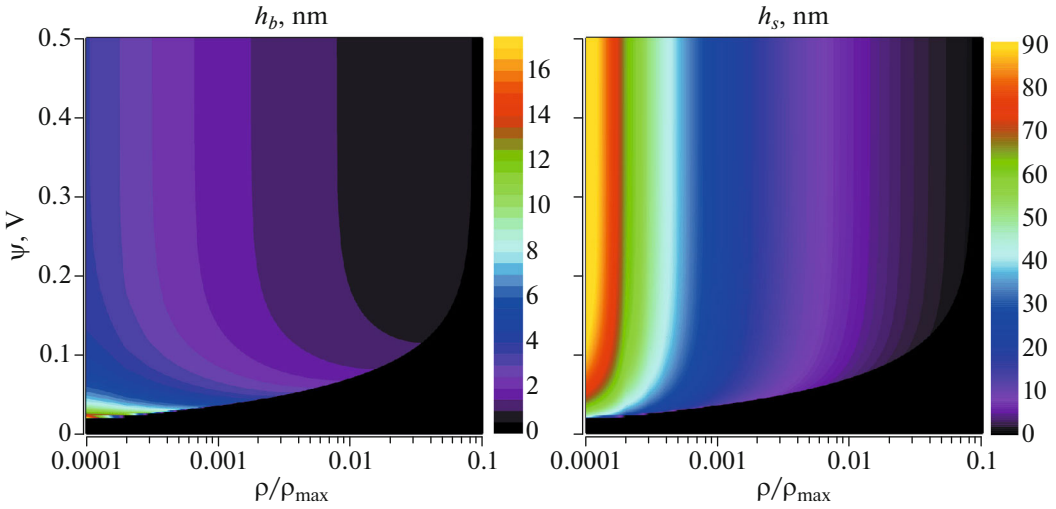

Fig. 3. The barrier position (left) and the secondary minimum position (right). Black color corresponds to the absence of secondary minimum and barrier (no metastable state available).

density and the Debye length λ_D. Other parameters are $\zeta_j = \tanh\left(\frac{zq_e\psi_j}{4kT}\right)$, where z is the valency of ions, $q_e = 1.6\times10^{-19}$ Q is elementary charge, ψ_j, $j = 1,2$ are electric potentials for each of two contacting surfaces, $\varepsilon_0 = 8.85\times10^{-12}$ F/m is absolute permittivity, ε is relative permittivity of a fluid with solute ions between solid surfaces. The maximum value of ion concentration is $\rho_{max} \sim 7\times10^{27}$ m^{-3} and corresponds to a strong salt solution.

The potential (5) is well known and was described in detail in many sources (e.g. [30, 38]). Therefore, we omit its detailed discussions. This potential has two minima with separation distances h_p and h_s and a barrier with $h = h_b$ for some ion concentrations and electric potentials. Rock, concrete and other porous materials widely used in industry contain a sufficient amount of fluid and ions between the grains even in room conditions to be trustworthy recorded in elastic moduli (e.g., the results of accurate measurements in [40]). Therefore, the potential (5) is a good approximation for better understanding of slow and fast time processes.

An example of (5) is shown in Fig. 2. The characteristic values of the separation distances are depicted by the labeled dashed lines. The upper plot in Fig. 2 shows the sign of the second derivative $V''(h)$. The areas for $V''(h) > 0$ are colored gray and correspond to the stability intervals where there is an attraction either to the main equilibrium or to the second minimum.

When discussing Fig. 1 we specified the conditions under which the broken contact moves to a metastable state. The results of the calculations of the potential (5) for various values of ρ and surface potential $\psi_1 = \psi_2 = \psi$ are shown in Fig. 3. Typical values of h corresponding to the barrier are $h_b \simeq 1$–10 nm, depending on ion concentration. Typical values of the distance between two surfaces for the secondary minimum are $h_s \simeq 5$–100 nm. Thus, if $h = -\delta_c > h_b$, some broken contacts can move to the attraction basin of the second minimum of (5) (see also the upper plot in Fig. 2). Otherwise, when $-\delta_c < h_b$ or the transition time to the second minimum of (5) is not small enough, the broken contact will be restored during the compression stage of excitation. This case corresponds to nonlinear hysteresis in the stress–strain relation or fast time phenomena in terms of [5].

4. MICROSCOPIC FLUCTUATIONS IN SLOW TIME PHENOMENA

For estimating the time of the transition to the secondary minimum the problem should be considered in more detail. The separation of two surfaces with adhesion is a dissipative process [37–39]. The equilibrium of surface interactions is mainly broken due to surface charges and discharges, as well as triboelectricity effects [38]. The presence of an electrolyte, which implies the potential (5), reduces the contribution of surface charges. But then ion movement becomes significant. In general, all changes in an adhesive layer should be referred to some kind of diffusion processes [38]. Therefore, as we don't know a real potential for surface interactions, we can presume the existence of diffusion processes without details concerning the corresponding kinetic phenomena. For kinetic phenomena with small changes of mean values in each elementary act of interaction (e.g., molecules impact), the kinetic equation is Fokker–Plank's equation [41].

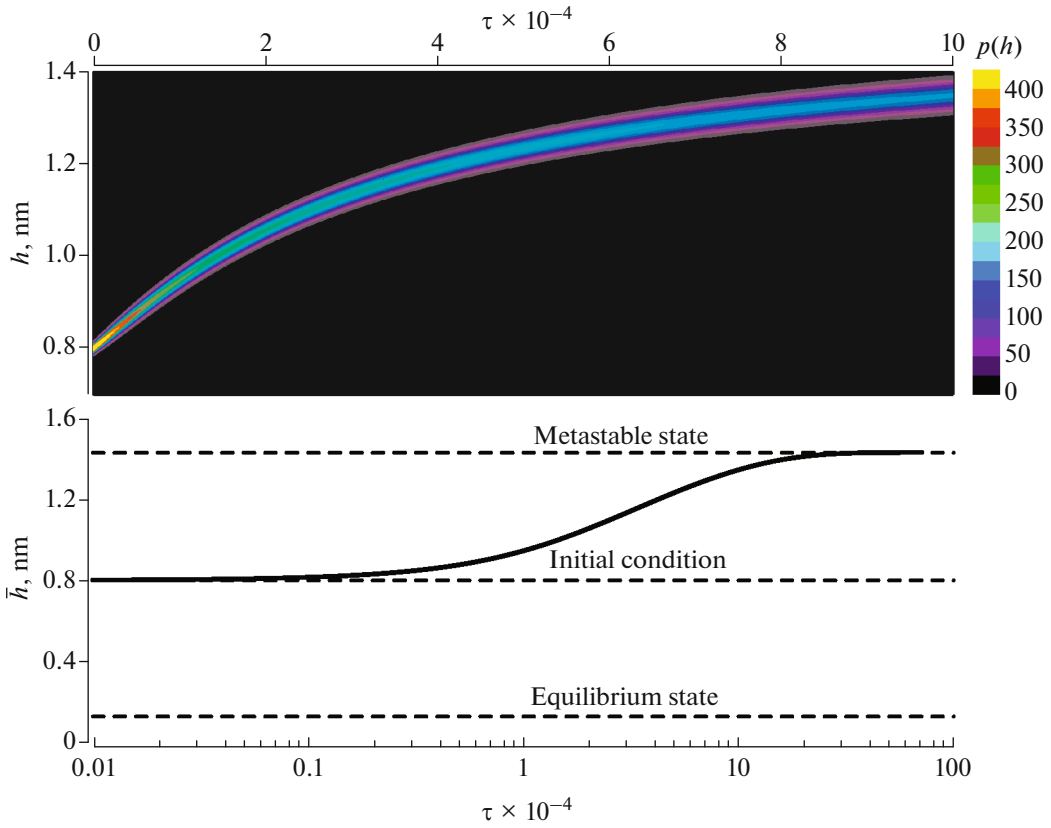

Fig. 4. Transition to metastable state.

As applied to the problem considered, this equation can be written in the form

$$\frac{\partial p(h,\tau)}{\partial \tau} = \left(\frac{U''(h)}{U''(h_p)}\right) p(h,\tau) + \left(\frac{U'(h)}{U''(h_p)}\right)\frac{\partial p(h,\tau)}{\partial h} + \frac{kT}{U''(h_p)}\frac{\partial^2 p(h,\tau)}{\partial h^2}. \quad (6)$$

Here, $p(h,\tau)$ is the probability density of states (e.g., ion concentration) for a specified separation distance between the surface, $\tau = t/\mathcal{T}_c$ is the dimensionless time, the potential $U(h)$ equals $V(h)S_{\text{eff}}$ and $S_{\text{eff}} = \pi a^2$ if the contact is not broken and $S_{\text{eff}} = 2\pi R h_0$, otherwise (see pages 143 and 162 in [30]). Equation (6) can be considered as a model one only because no details of kinetic phenomena are taken into account. Therefore, to exclude possible misunderstanding we consider the calculations as qualitative ones when this equation is used.

The normalizing time $\mathcal{T}_c$ is

$$\mathcal{T}_c = \frac{kT}{U''(h_p)D}\frac{1}{24\pi}\left(\frac{2}{9\pi}\right)^{2/3}\frac{kTh_p}{\gamma\mu DR}, \quad (7)$$

and corresponds to the time of the transition to the main state of equilibrium, when $|h - h_p| \ll h_p$ and $B = 0$ in (5). The numerical value on the right corresponds to the contact radius calculated for $F = 0$ in (2).

The value of $\mathcal{T}_c$ is proportional to the temperature and inversely proportional to the diffusion coefficient D, the curvature R, the adhesion coefficient γ, and the value of μ (1). All these dependences seem reasonable: if the adhesion effects are significant, the value of $\mathcal{T}_c$ decreases. For normal temperature of about 300 K and $R = 10^{-7}$ m, which corresponds to $\mu = 1$ for $\gamma = 0.1$ J/m^2 (quartz, glass), the value of $\mathcal{T}_c$ in seconds is estimated to be $\sim 10^{-26}/D$. The uncertainty is highest for the diffusion coefficient D, because no specific kinetic phenomena are considered for generality. According to the reference books, a typical value of the diffusion coefficient for transport phenomena in fluids is about $D \sim 10^{-9}$ m^2/s. The diffusion of salt ions in water at normal temperature and pressure is characterized by $D \sim 10^{-13}$ m^2/s. Even with such a large discrepancy in the value of D, we have a very small characteristic time $\mathcal{T}_c \sim 10^{-17}$–$10^{-13}$ s. Therefore, the product $\omega\mathcal{T}_c \ll 1$ for all known experimental data where slow

time phenomena have been observed. In this case, no terms describing an external source in the right-hand side of (6) are required. We can consider changes of $p(h,\tau)$ as a result of the initial perturbations with probability maximum at $h = -\delta_c$, when a contact has been broken and all transient processes have been accomplished.

The result of numerical integration of (6) is presented in Fig. 4. The parameters of (5) were set arbitrary for illustrative purposes: $\rho = 0.08\rho_{max}$ and $\psi = 0.5$ V. Values of the distances in nanometers for these parameters are: $h_p \approx 0.127$, $h_b \approx 0.646$, and $h_s \approx 1.432$. The initial distribution

$$p(h) = \frac{1}{\sqrt{2\pi\mathcal{D}_p}}\exp\left(-\frac{(h-\bar{h})^2}{2\mathcal{D}_p}\right), \quad (8)$$

was Gaussian with $\bar{h} = 0.8$ nm, which corresponds to the same value of $-\delta_c$ at the moment of contact break.

The Gaussian distribution describes typical microscopic fluctuations near the equilibrium state [42]. In the equilibrium state, the stationary distribution is Gaussian with $\bar{h} = h_p$ and the dispersion is $\mathcal{D}_p = kT/U''(h_p)$, which leads to a very small value of $\mathcal{D}_p \sim 10^{-10}h_p^2 \sim 10^{-30}$ m^2 for the main equilibrium state. Note that for the metastable state, the probability distribution is also of the Gaussian type with $\mathcal{D}_s = kT/U''(h_s)$ and $\bar{h} = h_s$. The main equilibrium state is much narrower compared to the metastable state (see Fig. 2); therefore, $\mathcal{D}_s \gg \mathcal{D}_p$.

After contact (bond) breaking the distribution was expected to have the same dispersion. Numerical integration of (6) for such small dispersion requires too many nodes for the spatial coordinate h, while no qualitative changes were observed in the solution. For this reason the dispersion was set $\mathcal{D} = 10^{-4}\bar{h}^2$ to allow fewer nodes in the spatial coordinate of (6). Figure 4 shows that the time of the transition to the secondary minimum is about $10^6\mathcal{T}_c$. Bearing in mind the above made evaluation of $\mathcal{T}_c$, the transition time is not more than 10^{-7} seconds. This is much less than the period of the conditioning signal used in all known experiments. It is also clearly seen that the dispersion $\mathcal{D}$ during the transition to the metastable state increases by virtue of the inequality $\mathcal{D}_s \gg \mathcal{D}_p$.

Therefore, we can describe the scenario of the arising metastable states. First, the metastable states are initiated by the instability of a contact with adhesion. This is due neither to the nonlinear effect of strain rectification, as was supposed in [25], nor to some kind of a frictional slip like that proposed in [15], although such a slip can be qualitatively considered in this way. Second, all further changes are due to the diffusion processes associated with a variety of transport phenomena (diffusion of ions, charges, etc.). Third, a broken bond moves to the metastable state under specific additional conditions only. Namely, after the fast instability process, the distance between the ruptured surfaces will be in the basin of attraction of the secondary minimum of surface potential. The time of the transition to the metastable state is small enough compared to the excitation periods. Therefore, the transition can be considered as an instant event.

The lifetime of the metastable state is determined by the exponent of the barrier height relative to the kinetic energy of thermal movements [43, paragraph 9.1.3] or (see paragraph 9.1.3 in [43]) or (see paragraph 9.1.3 in [43]):

$$\Delta t = \frac{kT}{Rh_0D}(|V''(h_b)|V''(h_s))^{-1/2} \times \exp\left(\frac{2\pi Rh_0(V(h_b)-V(h_s))}{kT}\right) = \mathcal{T}_0\exp\left(\frac{\Delta U}{kT}\right). \quad (9)$$

Here $V(h_b) > V(h_s)$ and h_b, h_s correspond to the positions of the barrier and the secondary minimum, and $\mathcal{T}_0$ is used for the substitution of the pre-exponential term in the first line of (9). Calculations of the potential (5) with $\rho = 0.05\rho_{max}$, $\psi = 0.5$ V and $\gamma = 0.1$ J/m^2 give the following relation: $\Delta U/kT = 2\times10^8 R$ and $\Delta U/kT \gg 1$ except very small values of the curvature radius $R \sim 10^{-8}$ m. The condition (1) for the same parameters leads to $\mu \sim 1$, which means that no hysteresis with bond breakage instability occurs (see also the discussion in [29]).

The transition through the barrier to the equilibrium state with $h = h_p$ is possible due to non-zero probability

$$p(h) = \frac{1}{\sqrt{2\pi\mathcal{R}_s}}\exp\left(-\frac{(h-h_s)^2}{2\mathcal{D}_s}\right), \quad (10)$$

at $h = h_p$. The probability distribution ((10)) describes microscopic fluctuations for the second minimum of the potential function $V(h)$ after external loading (conditioning) is switched off. Note that (10) corresponds to the equilibrium probability distribution and the condition $p(h_p) > 0$ is fulfilled due to microscopic fluctuations.

The relaxation process in this case can be interpreted as proposed by I. Prigogine for the description of chemical reactions with non-zero activation energy [44, 45]: when the kinetic energy of a molecule is higher than the activation energy (barrier), there occurs a reaction, after which the Maxwell distribution of molecule velocities becomes slightly non-equilibrium and relaxes to the equilibrium state, after which the process continues. In other words, a small fluctuation on the microscopic scale described by (10)

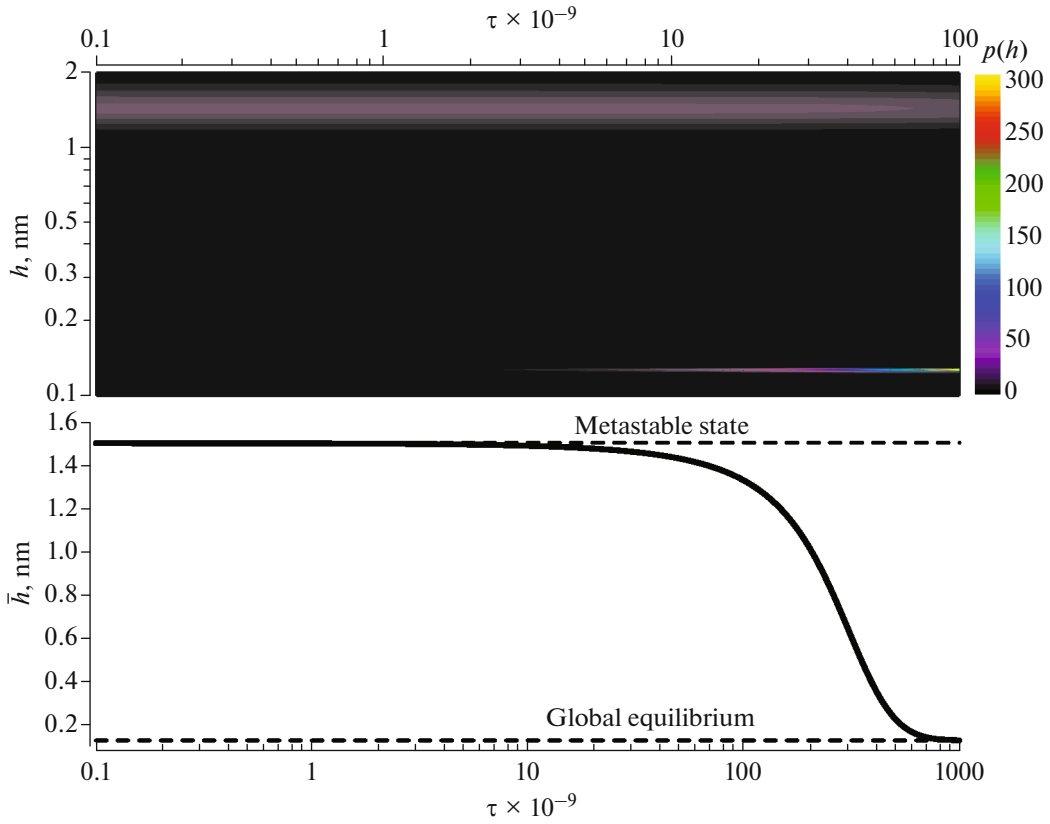

Fig. 5. Changes of probability distribution during slow relaxation (on top) and potential profile (at the bottom).

for a metastable state leads to the transition (10), brackets are redundant the main equilibrium state. The perturbations of (10), brackets are redundant are too small to consider this distribution as an almost equilibrium one because $p(h_p) \lll p(h_s)$.

Numerical integration of (6) demonstrates the scenario described above. The probability density evolution in the numerical solution of (6) is demonstrated in Fig. 5. The last term in (6) was multiplied by 10^4 to reduce the number of nodes in numerical integration and the corresponding computation time. Furthermore, the too narrow distribution of (10) corresponds to a numerically zero probability at $h = h_p$, even if double precision is used in calculations. Parameters of the potential (5) are the same as in Fig. 4. The evolution of $p(h)$ is clearly seen in Fig. 5. The initial normal distribution with maximum at $h = h_s$ (metastable state) slowly transforms to normal distribution with $h = h_p$ (equilibrium state). As the distribution dispersion $\mathcal{D}$ is inversely proportional to the second derivative of the surface forces potential $U''(h)$, the final distribution becomes narrower than the initial one. The population in metastable state decreases as a result of the transition to the global equilibrium state. The relaxation time is estimated to be $10^{16}\mathcal{T}_c$, with the diffusion correction taken into account. Note that $10^{16}\mathcal{T}_c \sim 10^3$ s is on the order of the relaxation time observed (e.g., [15]).

5. FLUCTUATIONS ON MESOSCOPIC SCALES: THE ORIGIN OF THE LOGARITHMIC TIME DEPENDENCE

In the previous section we have shown that the process of slow time relaxation originates on microscopic scales due to diffusion processes. Individual bond restoration can also be considered as a fluctuation if there exists an ensemble of bonds in metastable states. The fluctuation of this type is not microscopic and is related to mesoscopic scales. The term “mesoscopic” was proposed by our colleagues [5] for the interactions on the scale of grains, cracks, and the like in natural or artificial materials. If the number of detached bonds is large compared to unity within a representative volume but is small than the total number of bonds, the probability distribution of states is a limit of binomial distribution and is described as a Poissonian process [42, paragraph 114]. Slow time relaxation is a hierarchical process that is explained in Fig. 6. Ten traces of Brownian motion of particles (e.g., ions which are

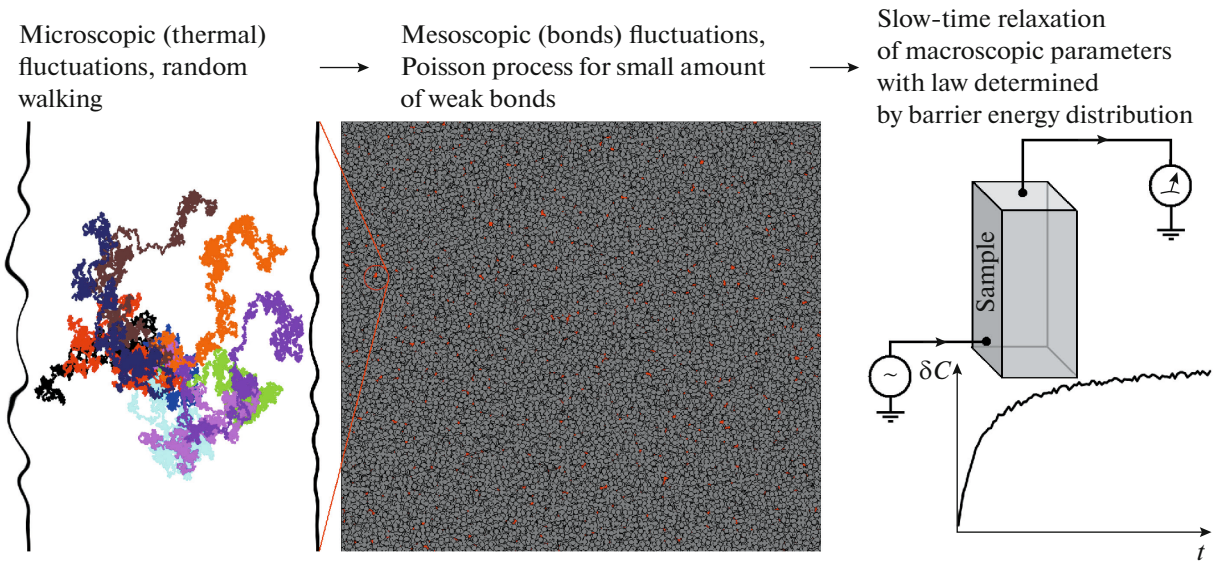

Fig. 6. Slow time relaxation as a hierarchical process: from thermal fluctuations on microscopic scales to bond fluctuations on mesoscopic scales.

more massive than the other molecules) are shown on the left. These scales are described by the Fokker–Plank equation (6) and two uneven surfaces become much closer at the end of the corresponding diffusion process. So, we now pass over to excited bonds. They are represented by the red voids in the center of Fig. 6. If the number of these excited bonds is very small compared to the total number of bonds in a heterogeneous material, they can also be described as a relaxation process. This relaxation process takes place on mesoscopic scale shown schematically in the center of Fig. 6. Finally, this process is revealed in the observed relaxation of macroscopic parameters as shown schematically in the right part of Fig. 6, where a typical measurement scheme and a relaxation graph are depicted. Now we will show why the logarithmic dependence arises if some additional requirements to barrier energy values are satisfied.

For the Poissonian process, the probability that there was no transition from the metastable to the stable state is

$$\frac{dP_0(t)}{dt} = -\xi P_0(t), \quad P_0(t) = \exp(-\xi t), \tag{11}$$

where ξ is the probability of the event within an infinitely short time interval t, $t + dt$. The quantity ξ is the velocity of the transition from the metastable to the stable state over an infinitely short time interval dt. This quantity is defined by the Arrhenius equation [43, 45], which is the other side of the consequence of the solution (9) of Fokker–Plank equation (see also equation 5.2.174 in [43] and the discussion therein):

$$\xi = \frac{1}{\mathcal{T}_0}\exp\left(-\frac{\Delta U}{kT}\right). \tag{12}$$

Therefore, to evaluate variations of the elasticity modulus M, the integration over all possible ΔU is required. The values of U_s do not significantly differ from zero (Fig. 2) and, hence, $\Delta U \approx U_b$. As a result, the relative change of the modulus or the modulus defect is

$$\frac{\Delta M}{M_0} = -\frac{1}{U_2 - U_1}\int_{U_1}^{U_2} P_0(U,t)\, dU, \tag{13}$$

where U is the barrier energy, depending on ion density and surface electric potential in (5), $U_1 = \min U$, $U_2 = \max U$, and M_0 is the unperturbed value of the modulus. Equation (13) implicitly presumes that metastable states with $h > h_p$ make bonds weaker and $\Delta M < 0$.

Using (12) the quantity dU can be expressed as $dU = -\frac{kT}{\xi}d\xi$. After the substitution into the integral (13) we obtain

$$\begin{aligned}\frac{\Delta M}{M_0} &= \frac{kT}{U_2 - U_1}\int_{\xi(U_1)}^{\xi(U_2)} P_0(\xi)\frac{\exp(-\xi t)}{\xi}d\xi \\ &= -\frac{kT}{U_2 - U_1}P_0(U_c)[E_1(\xi_1 t) - E_1(\xi_2 t)],\end{aligned} \tag{14}$$

where $\xi_1 = \xi(U_2)$, $\xi_2 = \xi(U_1)$ are the minimal and maximal values of ξ, $E_1(x) = \int_x^\infty \frac{e^{-\chi}}{\chi}d\chi$ is the integral exponential function [46], and $U_1 \le U_c \le U_2$ is the characteristic energy. The substitution of $P_0(U)$ with

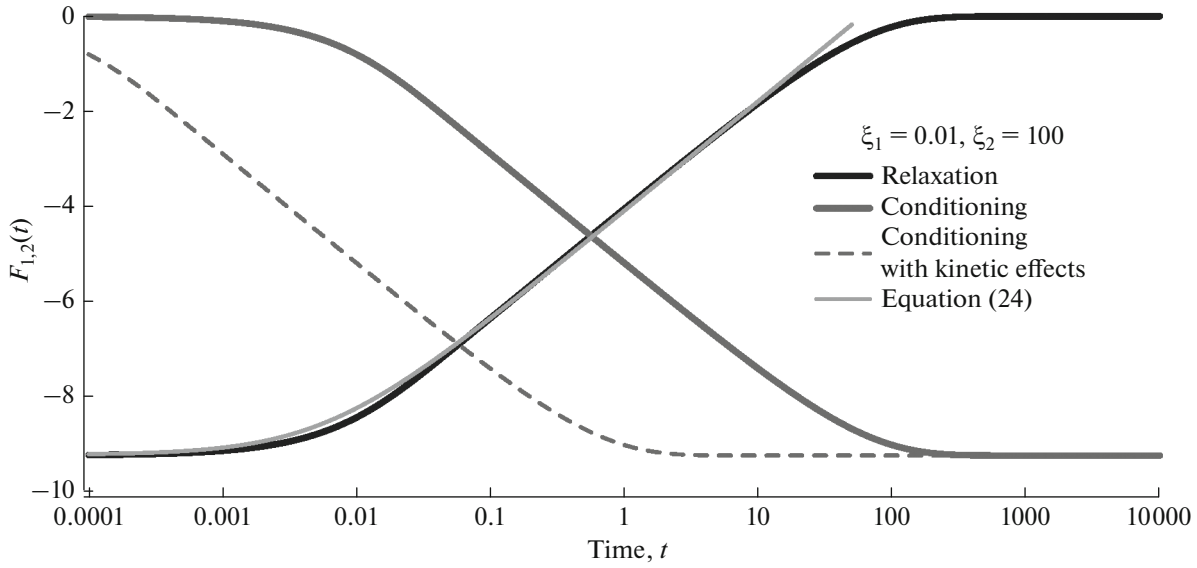

Fig. 7. Modulus defect versus time at conditioning and relaxation stages. The solid light-gray line is discussed in Section 6.

$P_0(U_c)$ is possible if $P_0(U)$ is a function that is smooth compared to the exponential functions in the integrand, so in this case $U_c \simeq (U_2 - U_1)/2$.

Mathematical properties and tables for integral exponential functions are available in [46]. For a very small argument, $\lim_{x\to 0} \mathrm{E}_1(x) = -\mathscr{C} - \ln x$, where $\mathscr{C} \approx 0.577$ is the Euler constant. At the beginning of relaxation $\xi_{1,2}t \ll 1$; therefore, the initial value of the modulus defect is

$$\frac{\Delta M}{M_0} = -\frac{kT}{U_2 - U_1} P_0(U_c) \ln\left(\frac{\xi_2}{\xi_1}\right) = -P_0(U_c). \qquad (15)$$

The term on the right corresponds to (12), and $P_0(U_c)$ characterizes a (small) part of metastable states. According to many experimental results, $\Delta M/M_0 \simeq -10^{-3}$ for the deformation amplitudes $\epsilon \sim 10^{-6}$–10^{-5}; therefore, $P_0(U_c) \simeq 10^{-3}$ as well.

The characteristic energy U_c obviously depends on $U_{1,2}$, while $U_{1,2}$ depend on strain amplitude (see equations (3) and (4) above). For moderate strain amplitudes, we can use the Taylor expansion for U_c:

$$U_c(\epsilon) = U_c^{(0)} + \left.\frac{\partial U_c}{\partial \epsilon}\right|_{\epsilon=0} \epsilon + \mathbb{O}(\epsilon^2), \qquad (16)$$

where ϵ is the strain amplitude used in conditioning. The linear dependence $U_c(\epsilon)$ means also a linear dependence $P_0(U_c)$ because the function $P_0(U)$ was assumed to be smooth. Therefore, the modulus defect at the beginning of the relaxation process should be linearly dependent on the excitation strain amplitude. This dependence has been observed many times in experiments (see Fig. 7 in [47]). The quantity $U_c^{(0)}$ in (16) describes the experimentally observed threshold for the slow time relaxation initiation [29, 47] (see also Fig. 5 in [15]).

With increasing relaxation time, the value of $\xi_2 t$ becomes larger than unity. For a large argument, $\lim_{x\to\infty} \mathrm{E}_1(x) = 0$ and the modulus defect for the times $\xi_1 t \ll 1$ and $\xi_2 t \gg 1$ is

$$\frac{\Delta M}{M_0} = \frac{kT}{U_2 - U_1} P_0(U_c)(\mathscr{C} + \ln \xi_1 t). \qquad (17)$$

This time interval corresponds to the logarithmic dependence of $\Delta M(t)/M_0$. For the time interval $\xi_{1,2}t \gg 1$, both integral exponents in (14) are equal to zero and $\Delta M/M_0 = 0$, which corresponds to the end of the relaxation process. The overall duration of the relaxation process is on the order of $\sim 1/\xi_1 - 1/\xi_2$.

It is clearly seen from the equations considered above that the logarithmic relaxation law is specified by a wide spectrum of energy barrier values. Otherwise, if this spectrum is narrow, the exponential type of relaxation will be observed. This corresponds to equation (13) with $U_1 \simeq U_2$. Consequently,

$$\frac{\Delta M}{M_0} \simeq \frac{\Delta M|_{t=0}}{M_0} \exp(-\xi t), \text{ and}$$
$$\xi = \frac{1}{\mathscr{T}_0} \exp\left(-\frac{\Delta U}{kT}\right).$$

The relaxation process can be long enough, while the modulus defect relaxes exponentially.

5.1. Logarithmic Dependence at the Excitation Stage

According to the description presented above, both stages of conditioning and relaxation do not actually differ from each other. Let us consider the transition of some detached bonds with $-\delta_c \lesssim h_b$ through the barrier. In this case, the microscopic fluctuations give rise to a tail of distribution of the (8) type with $p(h)|_{h>h_b} > 0$, and during the extension phase of external excitation the broken contact can make a transition to the metastable state. Although ΔU values in (12) are expected to be lower than at the relaxation stage, at the beginning we will not distinguish between them for simplicity. This allows us to show time reversibility of both, conditioning and relaxation stages.

For the relaxation stage, it is reasonable to consider the probability of absence of the transition (11). For the conditioning stage, let us consider the opposite situation:

$$\widetilde{P}_0(t) = 1 - \exp(-\xi t). \tag{18}$$

By repeating the procedures (11)–(14) we obtain the following time dependence of the modulus defect:

$$\frac{\Delta M(t)}{M_0} = -\frac{kT}{U_2 - U_1} P_0(U_c) \times [\mathsf{E}_1(\tilde{\xi}_2 t) + \ln(\tilde{\xi}_2 t) - \mathsf{E}_1(\tilde{\xi}_1 t) - \ln(\tilde{\xi}_1 t)]. \tag{19}$$

The integral expression (see Eq. 5.1.39 in [46])

$$\int_0^x \frac{1 - \exp(-z)}{z} dz = E_1(x) + \ln(x) + \mathscr{C},$$

is used to derive (19).

It is seen that at $t = 0$ all values in the square brackets in (19) cancel each other and $\Delta M(0)/M_0 = 0$. In the limiting case $t \to \infty$, the integral exponential functions approach zero and the modulus defect value coincides with (15). The qualitative evolution of the modulus defect for both conditioning and relaxation stages is shown in Fig. 7. The solid black and gray lines were calculated for $\tilde{\xi}_1 = \xi_1$ and $\tilde{\xi}_2 = \xi_2$. Values of $\xi_{1,2}$ were set arbitrary to show the trends in Fig. 7. The function $F_1(t)$ is identical to the expression in square brackets in (14) and to the analogous expression in (19). It is seen that both $F_1(t)$ and $F_2(t)$ are the same within time reversing and the processes of conditioning and relaxation are reversible.

The logarithmic time dependence at the conditioning stage, described mathematically above, can be treated from a physical standpoint. If the value of $-\delta_c$ is slightly less than the barrier position h_b, the "tail"of the distribution (8) is in the attraction basin of the second minimum. During each excitation (conditioning) period, some microscopic fluctuated states are attracted to this minimum. This corresponds to the same tunnel effect as for the relaxation stage. It is clear that, in general, the $\tilde{\xi}_{1,2}$ values are not equal to $\xi_{1,2}$. The difference $U_2 - U_1$, which is treated as the difference of the barrier heights at the pumping stage (19), is not equal to that for relaxation (14). Still another difference between the conditioning and relaxation stages is due to the kinetic energy (strain rate) contribution.

To account for kinetic energy we need to re-examine (12). When slow time relaxation is observed, the probe wave amplitude used for $\Delta M/M_0$ measurements is very small. In this case, the quantity ΔU is determined by the internal structure only (sizes of asperities, adhesion coefficient, etc.) and no perturbations of (5) occur. During conditioning, strain amplitudes can't be considered small and the potential (5) is perturbed by the kinetic energy of motion resulting from external loading (conditioning). Simple considerations based on the Bernoulli equation for a fluid flow [24], point to pressure reduction in the contact area by $\varrho v^2/2$, where ϱ is the density of the fluid and v is the fluid flow velocity. The quantity $\varrho v^2/2$ is a kinetic energy per unit volume. The pressure reduction means that the repulsive forces due to a double electric layer (the term proportional to B) in (5) decrease. As a result, the barrier height decreases too and (12) may be rewritten in the form

$$\xi = \frac{1}{\mathscr{T}_0} \exp\left(-\frac{\Delta U - \mathscr{E}}{kT}\right), \tag{20}$$

where $\mathscr{E}$ is the kinetic energy for the representative volume in the contact area. The values of $\tilde{\xi}_{1,2}$ become less than $\xi_{1,2}$ and equation (19) describes a faster process than that for the relaxation stage. This is illustrated by the dashed gray curve in Fig. 7. The time dependence of $\Delta M/M_0$ at the conditioning stage explains the observed dependence of slow relaxation parameters on the excitation time [47] (see also Fig. 4 in [48]). If conditioning is insufficiently long, not all barrier energies are excited. In this case, the difference $U_2 - U_1$ in (14) becomes less than it could be. Presumably this fact can explain two slopes in the logarithmic relaxation which were observed in [49] and detected in [47].

The curves shown by the gray lines in Fig. 7 are not easy to measure because during conditioning the modulus defect is caused not only by the slow time process but primarily by the fast time process (modulus perturbation due to nonlinear hysteresis). The hysteresis produces disturbances $\Delta M/M_0 \sim 10^{-2}$–$10^{-1}$ which are much larger than the residual value of $\Delta M/M_0 \sim 10^{-3}$ typical for slow time relaxation. A transient process with logarithmic dependence on time has been observed in one series of our experiments [18]. Due to deficient confidence of the data obtained we did not include them in the article [18], but it is worthy of notice that the time needed to reach

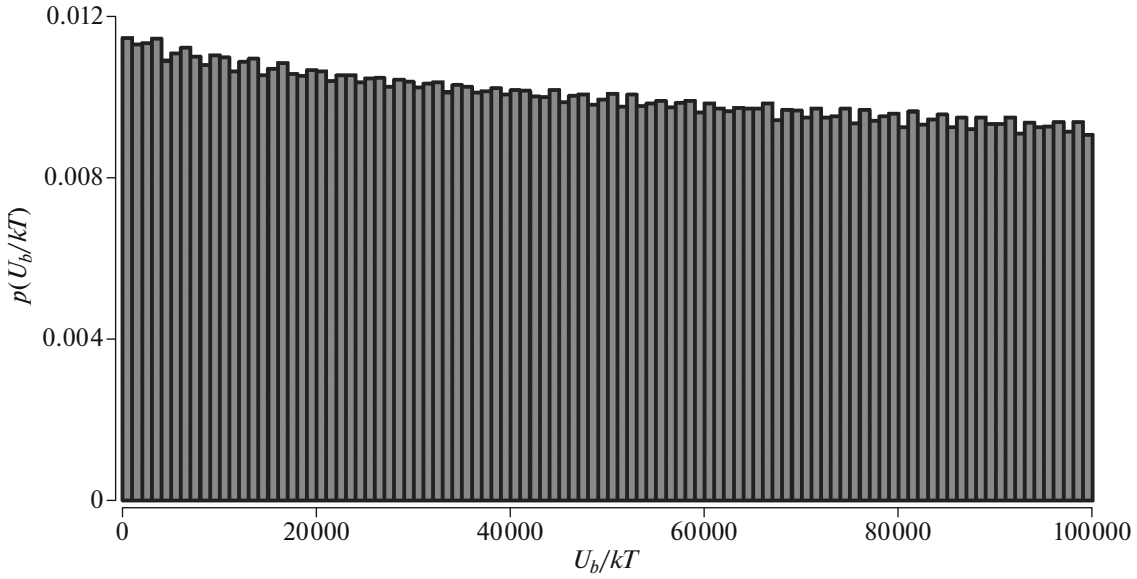

Fig. 8. Histogram of the distribution of $\Delta U/kT$ for the parameter variation shown in Fig. 3.

a saturated value of the modulus defect was much shorter than the time of relaxation. The correlation between the conditioning and relaxation processes was noted in [27]. In Fig. 3 of this paper one can see that conditioning is significantly faster than relaxation. This is in a qualitative agreement with the kinetic effects considered above and the mentioned difference $U_2 - U_1$ for the conditioning stage. However, the illustrations presented in [27] cannot be used to reveal the logarithmic dependence at the conditioning stage.

It is hard to make a correct theoretical estimation of $\mathscr{E}$ in (20) because of many ambiguities. In our opinion, the most appropriate way is to study kinetic effects in experiments, where the strain amplitude is fixed, while the frequency is variable. In this case, information on the dependence of relaxation parameters on strain rate could be obtained. To the best of our knowledge, no such experiments have been performed yet.

5.2. Smoothness of Barrier Energy Distribution

As seen from (14), the universality in the logarithmic time dependence of relaxing elastic moduli originates from the smooth and wide distribution of the barrier energies. The probability distribution of barrier energies for the potential (5) for the parameter variation shown in Fig. 3 is depicted in Fig. 8. The plotted histogram was calculated as follows. We set limiting values of $0 < \rho < \rho_{max}$ and $0 < \psi < 0.5$ V with small increments for each parameter. Then for each parameter combination, the energy of the barrier, if any, was recorded (about 10^6 individual values of barrier energies). Finally, all the found values were sorted in ascending order to plot the distribution presented in Fig. 8.

We see that the probability to find barrier energy in the interval $(10^0 \ldots -10^5)kT$ is almost uniform and smooth. Therefore, our presumption that the probability $P_0(U)$ in the integrand (14) is smooth enough for rewriting the integral with $P_0(U_c)$ multiplier, was correct. Thus, we can conclude that for all heterogeneous materials, where relaxation with logarithmic time dependence of the key parameter is observed, the potential of the interaction of structural elements will have an early uniform distribution of barrier heights. Furthermore, if some deviation from the logarithmic time dependence is observed, this points to non-uniformity of barrier energy distribution and can be used as a diagnostic tool in materials science. From this point of view, we intend to re-examine our conditioning results in [47, 48] in the near future.

DISCUSSION

As was pointed in the Introduction, Ref. [15] was the first article where slow time relaxation was explained. Curiously, the coefficient of the logarithm of time in this paper formally coincides with $\frac{kT}{U_2 - U_1}$ in (14). The explanation in [15] implied a general description of tunnel effects through the energy barrier without detailed specification and discussion of the physical nature of these barriers. Thus, we can conclude that although our colleagues made only a generic description, their model is a good one, taking into account additional considerations made in the paper presented. Refs. [19, 20] mentioned in the

Introduction are based on the results of [15]. It was stated in [19] that in the transition from one equilibrium state to another, three stages are distinguished for viscosity or any other internal parameter. This statement is in a good agreement with the function $F_1(t)$ in Fig. 7, where three stages are also well seen. The first one corresponds to $\xi_{1,2}t \ll 1$, the second to $\xi_1 t \ll 1$ and $\xi_2 t \gg 1$, and the third to $\xi_{1,2}t \gg 1$. The $F_1(t)$ curve looks qualitatively like that in Fig. 6 in [19]. We also see at least a qualitative agreement of the model proposed here with those proposed in [19, 20].

It is interesting to compare the expressions obtained above with the thermodynamic description of time-logarithmic relaxation made before in [16, 29, 47]. The basic assumption in this case was that the residual strain rate obeys the Arrhenius equation [44]:

$$\dot{\epsilon} = A\exp\left(-\frac{\Delta G}{kT}\right), \tag{21}$$

where ΔG is the Gibb's activation energy, and A is the pre-exponential multiplier slowly depending on temperature. The Gibb's potential is determined as $dG = Vdp - SdT$, where p is pressure, V is reference volume, and S is entropy. In the considerations presented below we assume that the temperature is invariable.

By taking a natural logarithm of both sides of (21) and differentiating over time we obtain the following equation:

$$\frac{\ddot{\epsilon}}{\dot{\epsilon}} = -\frac{1}{kT}\frac{d\Delta G}{dt} + \frac{M_0 V}{kT}\dot{\epsilon}, \tag{22}$$

where the expression on the right was obtained by the substitution $dp = -d\sigma$, and the stress was expressed using the unperturbed elastic modulus M_0 and strain ϵ: $d\sigma = M_0 d\epsilon$.

After integrating (22) twice the following equation for residual macroscopic strain dependence on time can be written:

$$\epsilon(t) = \epsilon(0) - \frac{\Lambda}{M_0}\ln\left(\frac{t+t_0}{t_0}\right), \tag{23}$$

where $\epsilon(0) > 0$ is the residual dilation strain at the beginning of relaxation, $t_0 = -\dfrac{\Lambda}{M\dot{\epsilon}(0)} > 0$, $\dot{\epsilon}(0) < 0$ is initial strain rate, and $\Lambda = kT/V$.

The relative change of the modulus M is

$$\frac{\Delta M(t)}{M_0} = \beta\epsilon(t) = \beta\epsilon(0)\left[1 - \frac{\Lambda}{M_0\varepsilon(0)}\ln\left(\frac{t+t_0}{t_0}\right)\right], \tag{24}$$

where $\beta < 0$ is the quadratic nonlinearity parameter [5–8] which links the change of modulus M due to volumetric expansion ϵ.

The value of t_0 in (24) can be evaluated by the order of magnitude as ξ_2^{-1}, where ξ_2 is defined by (12) for ΔU equal to the maximum barrier value U_2. The dependence (24) is depicted by the solid light-gray line in Fig. 7. For illustrative purposes, the parameters of this curve were set to be $\beta\epsilon(0) = -9.2$, $\dfrac{\Lambda}{M_0\epsilon(0)} = 1$, and $t_0 = 0.6\xi_2^{-1}$. It is clearly seen that both (14) and (24) lead to almost the same dependence, except for the final stage of relaxation, where a simple description becomes incorrect.

By comparing (24) with equation (14) obtained above we can conclude that

$$\beta\epsilon(0) = -P_0(U_c), \quad \frac{\Lambda}{M_0\epsilon(0)} = \frac{kT}{U_2 - U_1}. \tag{25}$$

The value of $P_0(U_c)$ is less or equal to unity because it is a probability and, therefore, we have the inequality $|\beta\epsilon(0)| \le 1$ which simply reflects applicability of classical nonlinearity in the transition from (23) to (24). Indeed, the Taylor expansion of the free energy of elastic deformation described by classical nonlinearity means small perturbations due to the higher order terms ϵ^2, ϵ^3, etc. In this case, a much stronger inequality is required $|\beta\epsilon(0)| \ll 1$; therefore, $P_0(U_c)$ will also be much less than unity. It was suggested to consider the quantity Λ as a material parameter (see Table 1 in [29] and the corresponding discussion therein) if the results of measurements are normalized to the same conditioning strain amplitude. The last equality in (25) confirms this suggestion.

It is easily seen that the derivation of the relaxation law from (21) to (24) is much simpler than presented in Sections 4 and 5 and leads to similar results. Thus, we can state that the description of slow time relaxation using a simple approach does not contradict the results presented in Sections 4 and 5.

Many contemporary materials, which are of great importance for industry (ceramics, concrete, some alloys), consist of grains or other structural elements [50]. As pointed above, nonlinear phenomena, including slow relaxation processes are of key importance for assessing internal bond interactions. To be sure in the correctness of the proposed model the equations presented above need to be verified. The most detailed experimental studies have been undertaken for rocks. Hence, we use the corresponding experimental data, although the theory presented above can be applied for other materials as well.

Equation (14) allows evaluating material properties, such as the dependence of surface energy on the separation distance between the grains. The combination of two integral exponential functions provides initial and final stages of the relaxation process. Fast recording is needed to detect the initial stage of long-term relaxation, which was done in [49]. Note that such a detection is not easy to implement. For example, very accurate measurements [15, 18] were made

with a great amount of averaging, which masked the initial relaxation stage. The initial stage of relaxation like the one shown in Fig. 7 was clearly depicted in Fig. 6 in [47]. Therefore, Eq. (14) seems to be correct.

According to (15), the initial perturbation $\Delta M/M_0 = -P_0(U_c)$. Relative changes in the elastic wave velocity $\Delta c/c_0$ (mainly compressional and also shear wave velocity were measured in [18]), where "c_0" denotes an unperturbed value. The relative change in the elastic modulus was twice the relative change of velocity. The relative change of the compressional velocity $\Delta c/c_0 = -1.4\times10^{-4}$ at the beginning of relaxation after excitation with the deformation amplitude $\epsilon \approx 6\times10^{-6}$ is shown in Fig. 6 of [47]. The data of Fig. 5 in [15] for the same material (Berea sandstone) correspond to the first readout of $\Delta c/c_0 = -1.4\times10^{-4}$ for the excitation deformation amplitude $\epsilon = 2.6\times10^{-6}$. The conditioning deformation amplitudes in [49] were twice those in [15], while the initial perturbation at the beginning of relaxation was almost the same. This implicitly confirms the proposed mathematical description of the conditioning stage (the gray line in Fig. 5). The excitation time in [49] was approximately 2–3 orders of magnitude shorter than in [15]. Therefore, conditioning was not fully accomplished and the initial perturbation became smaller than possible for the conditioning amplitude of deformation.

The coefficient of the logarithm of time is $\frac{kT}{U_2 - U_1}P_0(U_c)$ (17). This value was measured in [15] to be 2.4×10^{-5} for $\Delta c/c_0$ and should be doubled for $\Delta M/M_0$. The probability $P_0(U_c)$ is determined by the initial perturbation and can be estimated as $P_0(U_c) \simeq 3\times10^{-4}$. Therefore, the value of $U_2 - U_1$ is about

$$U_2 - U_1 \approx 10kT. \quad (26)$$

The relaxation time was evaluated above as $1/\xi_1 - 1/\xi_2$, where $\xi_{1,2}$ are defined by (12). The ξ_2/ξ_1 ratio determines the time of the end of relaxation divided by the time of the relaxation beginning. This value is about $10^{3.5} \approx 3200$ as measured in [15]. Neglecting the presumably weak dependence of the pre-exponential multiplier $1/\mathcal{T}_0$ on U_b in (12) we obtain $U_2 - U_1 \simeq 8kT$. With the above made assumption regarding the $1/\mathcal{T}_0$ multiplier, the estimation obtained is in a good agreement with (26). Other accurate measurements of slow relaxation are presented in [18]. The material studied was carbonate rock (building material used for paving and casing). The initial value of $\Delta c/c_0 = -2\times10^{-4}$ for the excitation amplitude of $\epsilon \approx 5\times10^{-6}$. The ratio of the relaxation end and beginning times is about 200. By repeating the operations described above it is possible to obtain $P_0(U_c) \simeq 4\times10^{-4}$, $U_2 - U_1 \approx 6kT$ and $U_2 - U_1 \simeq 5.3kT$ using the ξ_2/ξ_1 ratio. Therefore, the description of slow relaxation presented in this paper does not contradict at least the experimental data from two independent sources. In this case, we can use the proposed model to evaluate the parameters of contact energy profiles. Knowing the value of $\Delta M/M_0$ or $P_0(U_c)$ at the beginning of relaxation one can estimate the fraction of weak contacts inside a heterogeneous material. Thus, comparison with known experimental data shows that the proposed model opens up important opportunities for materials science, as coherent and comprehensive diagnostics of heterogeneous materials becomes possible.

CONCLUSIONS

1. The analysis made reveals a hierarchy of relaxation processes occurring on microscopic and mesoscopic scales, which result in slow time relaxation of material parameters observed on macroscopic scales.

2. Microscopic fluctuations are the origin of slow time phenomena on mesoscopic and macroscopic scales. These fluctuations are thermally activated and should be controlled by environmental parameters influencing the diffusion rate.

3. The universal logarithmic time dependence of relaxing parameters is described by mesoscopic fluctuations if the energy barrier spectrum is wide and smooth. Otherwise, a narrow spectrum leads to the exponential law of relaxation.

4. The previously overlooked issue of the transition of a heterogeneous medium to a metastable state has been resolved. Key factors have been determined and an analogy between conditioning and relaxation stages has been found, indicating reversibility of the conditioning and relaxation processes.

5. The proposed model provides an explanation of the dependence of relaxation parameters on time and conditioning amplitude. The kinetic effects have been revealed and analyzed for the first time to the best of our knowledge. A plan of future investigations has been proposed.

6. All the above pointed issues can be used for nondestructive material testing. The idea of using fast and slow phenomena to detect defects of various types was proposed earlier [11–14, 27]. We believe that the proposed model makes diagnostics more coherent and comprehensive.

ACKNOWLEDGMENTS

The work was supported by the Russian Science Foundation (grant number 22-22-00230). The author is grateful

to Dr. A.A. Abrashkin for helpful comments and discussions on the topic of the article.

CONFLICT OF INTEREST

The authors declare that they have no conflicts of interest.

OPEN ACCESS

REFERENCES

1. J. F. Bell, in *Encyclopedia of Physics,* Ed. by C. Truesdell and S. Flügge (Springer-Verlag, Berlin, Heidelberg, New York, 1973), Vol. VIa/1.
2. R. N. Thurston and K. Brugger, Phys. Rev. **133**, 1604 (1964).
3. K. Brugger, Phys. Rev. **133**, 1611 (1964).
4. M. A. Breazeale and J. Philip, in *Physical Acoustics, Principles and Methods,* Ed. by W. Mason and R. Thurston (Acad. Press, 1984), **Vol. 17**, p. 2.
5. R. A. Guyer and P. A. Johnson, *Nonlinear Mesoscopic Elasticity: the Complex Behaviour of Rocks, Soil, Concrete* (Wiley-VCH, 2009).
6. K. A. Naugolnykh and L. A. Ostrovsky, *Nonlinear Wave Processes in Acoustics* (Cambridge Univ. Press, New York, 1998).
7. O. V. Rudenko and S. I. Soluyan, *Theoretical Foundations of Nonlinear Acoustics* (Plenum, Consultants Bureau, New York, 1977).
8. L. A. Ostrovsky and P. A. Johnson, Riv. Nuovo Cimento **24**, 1 (2001).
9. O. V. Rudenko, Phys.-Usp. **46**, 77 (2006).
10. R. A. Guyer and P. A. Johnson, Phys. Today **52**, 30 (1999).
11. K. V. D. Abeele, P. A. Johnson, and A. M. Sutin, Res. Nondestr. Eval. **12**, 17 (2000).
12. K. V. D. Abeele, A. Sutin, J. Carmeliet, and P. Johnson, NDT&E Int. **34**, 239 (2001).
13. M. Sclerandi, V. Agostini, P. Delsanto, K. V. D. Abeele, and P. Johnson, J. Acoust. Soc. Am. **113**, 3049 (2003).
14. P. Johnson and A. M. Sutin, J. Acoust. Soc. Am. **117**, 124 (2005).
15. J. A. TenCate, E. Smith, and R. Guyer, Phys. Rev. Lett. **85**, 1020 (2000).
16. V. S. Averbakh, A. V. Lebedev, A. P. Maryshev, and V. I. Talanov, Acoust. Phys. **55**, 211 (2009).
17. T. Brunet X. Jia, and P. A. Johnson, Geophys. Res. Lett. **35**, L19308 (2008).
18. V. S. Averbakh, V. V. Bredikhin, A. V. Lebedev, and S. A. Manakov, Acoust. Phys. **63**, 346 (2017).
19. M. A. Mironov, I. A. Shelomikhina, O. M. Zozulya, and I. B. Esipov, Acoust. Phys. **58**, 117 (2012).
20. I. B. Esipov, O. M. Zozulya, and M. A. Mironov, Acoust. Phys. **60**, 169 (2014).
21. Z. Peng and Y. Ben-Zion, Pure Appl. Geophys. **163**, 567 (2006).
22. F. Brenguier, M. Campillo, C. Hadziioannou, N. Shapiro, R. Nadeau, and E. Larose, Science **321**, 1478 (2008).
23. C. Wu, A. Delorey, F. Brenguier, C. Hadziioannou, E. G. Daub, and P. Johnson, Geophys. Res. Lett. **43**, 6129 (2016).
24. L. D. Landau and E. M. Lifshitz, *Course of Theoretical Physics,* **Vol. 6**: *Fluid Mechanics,* 2nd ed. (Pergamon Press, 1987).
25. V. Zaitsev, V. Gusev, and B. Castagnede, Phys. Rev. Lett. **90**, 075501 (2003).
26. V. Y. Zaitsev, V. E. Gusev, V. Tournat, and P. Richard, Phys. Rev. Lett. **112**, 108302 (2014).
27. M. Scalerandi, C. Mechri, M. Bentahar, A. Di Bella, A.S. Gliozzi, and M. Tortello, Phys. Rev. Appl. **12**, 044002 (2019).
28. D. Pasqualini, K. Heitmann, J. A. TenCate, S. Habib, D. Higdon, and P. A. Johnson, J. Geophys. Res. **112**, B01204 (2007).
29. A. V. Lebedev and L. A. Ostrovsky, Acoust. Phys. **60**, 555 (2014).
30. J. Israelachvili, *Intermolecular and Surface Forces* (Acad. Press, New York, 1992).
31. B. Lawn, *Fracture of Brittle Solids,* 2nd ed. (Cambridge Univ. Press, 1993).
32. R. A. Guyer, K. R. McCall, and G. N. Boitnott, Phys. Rev. Lett. **74**, 3491 (1995).
33. D. Maugis, J. Colloid Interface Sci. **150**, 243 (1992).
34. L. D. Landau, E. M. Lifshitz, A. M. Kosevich, and L. P. Pitaevskii, *Course of Theoretical Physics,* Vol. 7: *Theory of Elasticity* (Pergamon, New York, 1986).
35. N. Burnham and A. Kulik, in *Handbook of Micro/Nano Tribology,* Ed. by B. Bhushan, 2nd ed. (CRC Press LLC, Boca Raton, 1999), p. 263.
36. K. Johnson, K. Kendall, and A. Roberts, Proc. R.Soc. London A **324**, 301 (1971).
37. D. Maugis and M. Barquins, J. Phys. D: Appl. Phys. **11**, 1989 (1978).
38. B. V. Derjaguin, N. V. Churaev, and V. M. Muller, *Surface Forces* (Springer Sci., 1987).
39. J. Fineberg and M. Marder, Phys. Rep. **313**, 1 (1999).
40. V. S. Averbakh, V. V. Bredikhin, A. V. Lebedev, and S. A. Manakov, Acoust. Phys. **S56**, 794 (2010).
41. E. M. Lifshitz and L. P. Pitaevskii, *Course of Theoretical Physics,* Vol. 10: *Physical Kinetics* (Elsevier Sci., 1995).
42. L. D. Landau and E. M. Lifshitz, *Course of Theoretical Physics,* Vol. 5, Part 1: *Statistical Physics,* 3rd ed. (Elsevier, 1980).

43. C. Gardiner, *Handbook of Stochastic Methods for Physics, Chemistry and the Natural Sciences,* 2nd ed. (Springer, 1985).

44. D. Kondepudi and I. Prigogine, *Modern Thermodynamics. From Heat Engines to Dissipative Structures* (John Wiley & Sons, New York, 1998).

45. W. Stiller, *Arrhenius Equation and Non-Equilibrium Kinetics* (BSB B. G. Teubner Verlagsgesellschaft, Leipzig, 1989).

46. W. Gautschi and W. F. Cahill, in *Handbook of Mathematical Functions with Formulas, Graphs and Mathematical Tables,* Ed. by M. Abramowitz and I. Stegun (Dover, New York, 1964), p. 227.

47. L. Ostrovsky, A. Lebedev, J. Rivière, P. Shokouhi, C. Wu, M. A. Stuber Geesey, and P. A. Johnson, J. Geophys. Res.: Solid Earth **124**, 5003 (2019).

48. L. Ostrovsky, A. Lebedev, S. Manakov, J. Rivière, P. Shokouhi, R. Guyer, M. S. Geesey, and P. Johnson, Proc. Meet. Acoust. **34**, 032002 (2018).

49. P. Shokouhi, J. Rivi`ere, R.A. Guyer, and P.A. Johnson, Appl. Phys. Lett. **111**, 251604 (2017).

50. M. Ashby, *Materials Selection in Mechanical Design,* 2nd ed. (Butterworth-Heinemann, Oxford, 1999).